

Continuous hoops for transverse reinforcement of reinforced concrete columns

*Tae-Sung Eom¹⁾, Hong-Gun Park²⁾, Su-Min Kang³⁾,
Jong-Min Jin⁴⁾ and Hyoung-Bum Ahn⁵⁾

¹⁾ Dept. of Architectural Engineering, Dankook Univ., Kyeonggi 448-701, Korea

²⁾ Dept. of Architecture, Seoul National Univ., Seoul 151-742, Korea

³⁾ Architectural Engineering & Research Team, Daelim Co., Seoul 110-732, Korea

⁴⁾ New Business Team, Daehan Staz, Seoul 110-732, Korea

⁵⁾ Dept. of Architectural Engineering, Dankook Univ., Kyeonggi 448-701, Korea

¹⁾ tseom@dankook.ac.kr

ABSTRACT

A re-bar fabrication method using continuously wound rectangular or polygonal ties (or continuous hoops) was developed to enhance constructability and economy of reinforced concrete columns. In the present study, cyclic tests were performed to investigate the structural performance of the columns with continuous hoops. The test parameters were the shape, spacing, and bar-diameter of the continuous hoops, and the tolerance between the longitudinal bars and the tie hoops. The load-carrying capacity, deformation capacity, and failure mode of the specimens were directly compared with those of the columns with conventional ties. On the basis of the test results, the effect of the continuous ties was evaluated. Further, the spacing requirement of transverse reinforcement was studied to restrain the post-yield buckling of longitudinal bars in the plastic hinge.

1. INTRODUCTION

Current design codes such as ACI 318-11(2011) and KCI 2012 (2012) require strict transverse reinforcement details for the earthquake design of reinforced concrete beams, columns, and beam-column connections. The transverse reinforcement details are complicated by the use of close spacing, crossties, and 135-degree seismic hooks. Thus, the fabrication of re-bar cages requires elaborate efforts and construction time even for skilled workers (see Fig. 1(a)).

To ease the complicate re-bar work, various re-bar fabrication methods have been considered. Particularly, in Europe, the use of welded meshes, welded bar cages, and spirals has been increased for the transverse reinforcement of beams, columns, and walls. Recently, continuously wound ties (or continuous hoops) in the form of polygonal

^{1) 2)} Professors

^{3) 4)} Depute department heads

⁵⁾ Graduate student

helixes (i.e. rectangle, hexagon, octagon, etc.) was developed by using coiled bars and bending-and-cutting machines (Riva 2009, Fascia et al. 2010). For easy shipping, the continuous hoops are compressed and tied after fabrication. In construction site, the compressed continuous hoops are released in position (see Fig. 1(b)).

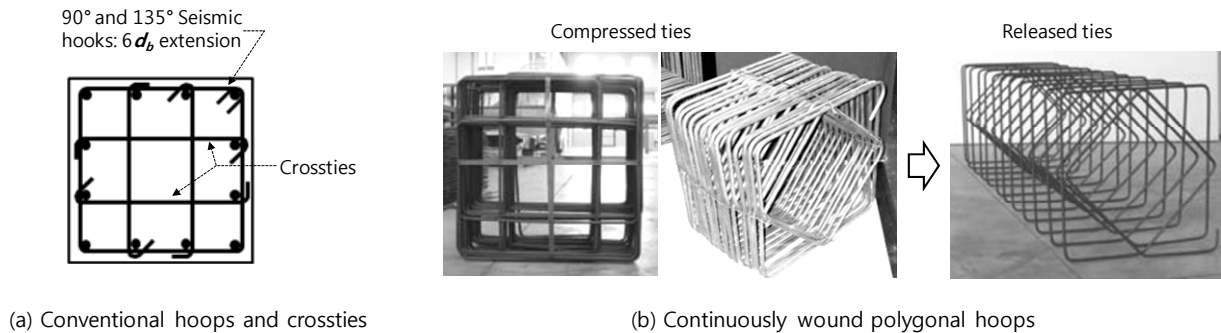


Fig. 1 Transverse reinforcement of reinforced concrete columns

When compared to conventional hoops using crossties and hook anchorages, the continuous hoops have several advantages. The construction time can be reduced because the ties enclosing longitudinal bars can be installed by simply releasing the compressed continuous hoops, as shown in Fig. 1(b). Various tie shapes including rectangular, T-shaped, hexagonal, and octagonal ones can be fabricated without difficulty. Furthermore, since hook anchorages are not necessary, the amount of coiled bars required for the ties can be decreased and re-bar congestion can be alleviated. From the viewpoint of structural safety and design, the continuous hoops are reliable particularly under cyclic loading because there is no risk of unfolding of the hook anchorages. Because of the continuity of the continuous hoops, the confinement effect may be better than that of the conventional ties. Furthermore, since 135-degree hook anchorages are not necessary, longitudinal bars can be concentrated at the corners of the rectangular ties, which can increase the flexural capacity of columns. On the other hand, a clearance between the longitudinal bars and ties is required to install the continuous hoops through the longitudinal bars. Because of the clearance, the structural capacity of the continuous hoops and the columns can be decreased. In the present study, the structural capacity of the continuous hoops was studied. Column specimens with the continuous hoops were tested under cyclic lateral loading. The structural performance including the load-carrying capacity, deformation capacity, and energy dissipation capacity was directly compared with the specimen with conventional hoops. From the test results, the effect of the shape and spacing of the continuous hoops was investigated. Further, the effect of the clearance between the longitudinal bars and ties was studied.

2. SHAPES AND DETAILS OF CONTINUOUS HOOPS

Fig. 2 shows three representative details of the continuous hoops for small to large size

columns: for small size cross-sections, rectangular hoop can be used (see Detail A of Fig. 2(b)); and for large size cross-sections with many longitudinal bars, rectangular-rhombic or rectangular-octagonal hoops can be used (see Details B and C of Fig. 2(b)). The rhombic and octagonal hoops replace the crossties of the conventional ties. The shape of the continuous hoops can vary according to the shape of the cross section and the arrangement of the longitudinal bars. At the ends of the continuous hoops, a seismic hook or one additional turn of hoop is needed for anchorage (ACI 318, 2011).

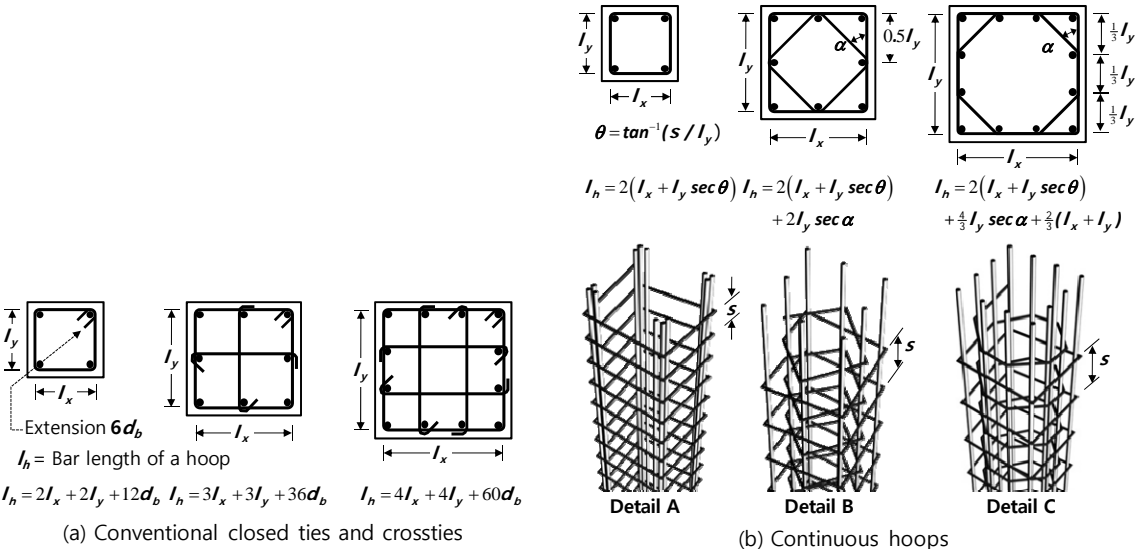


Fig. 2 Details of continuous hoops for columns

Table 1 Bar lengths per hoop of conventional ties and continuous hoops (mm)

Hoop dimension $I_x \times I_y$	Bar diameter d_b	Continuous hoops		Conventional tie	Ratio I_h/I_h'
		Hoop shape	Bar length per hoop I_h	Bar length per hoop I_h'	
Small 300x300	10	Detail A (Fig. 2):	1209	1320	0.916
	13	recangular	1209	1356	0.892
Medium 400x400	10	Detail B(Fig. 2):	2737	2760	0.992
	13	rectangular-rhombic	2737	2868	0.954
Large 500x500	10	Detail C(Fig. 2):	3620	4600	0.787
	13	rectangular-octagonal	3620	4780	0.757

Since the hook anchorage is not necessary, the quantity of the continuous hoops can be decreased. Table 1 compares the bar lengths per hoop, I_h , of the conventional ties (including crossties) and the continuous hoops. For the continuous hoops, three tie

shapes in Fig. 2(b) were used: Details A (rectangular hoop), B (rectangular-rhombic hoop), and C (rectangular-octagonal hoop). The conventional ties corresponding to the Details A, B, and C of the continuous hoops are shown in Fig. 2(a). The bar lengths were calculated for the bar diameter $d_b = 10$ and 13 mm, dimensions $l_x = l_y = 300, 400,$ and 500 mm, and spacing $s = 0.25l_x$ (or $\theta = 7.13^\circ$). The quantities of the ties (or the bar length per hoop) were decreased by 8.4 to 10.8 %, 0.8 to 4.6 %, and 21.3 to 24.3 % for the Details A, B, and C, respectively. As the number of the crossties increased in the conventional ties, the reduction in the quantity of the continuous hoops increased.

3. TEST PROGRAM

Four column specimens including a specimen with conventional ties were prepared for cyclic lateral loading test. Fig. 3 shows the configurations, reinforcement details, and cross sections of the specimens. Test parameters were the bar diameter, spacing, and hoop shape of the continuous hoops (see Table 2). The net column height from the critical section to the lateral loading point was 1500 mm. The dimension of the cross sections was 500 mm x 500 mm.

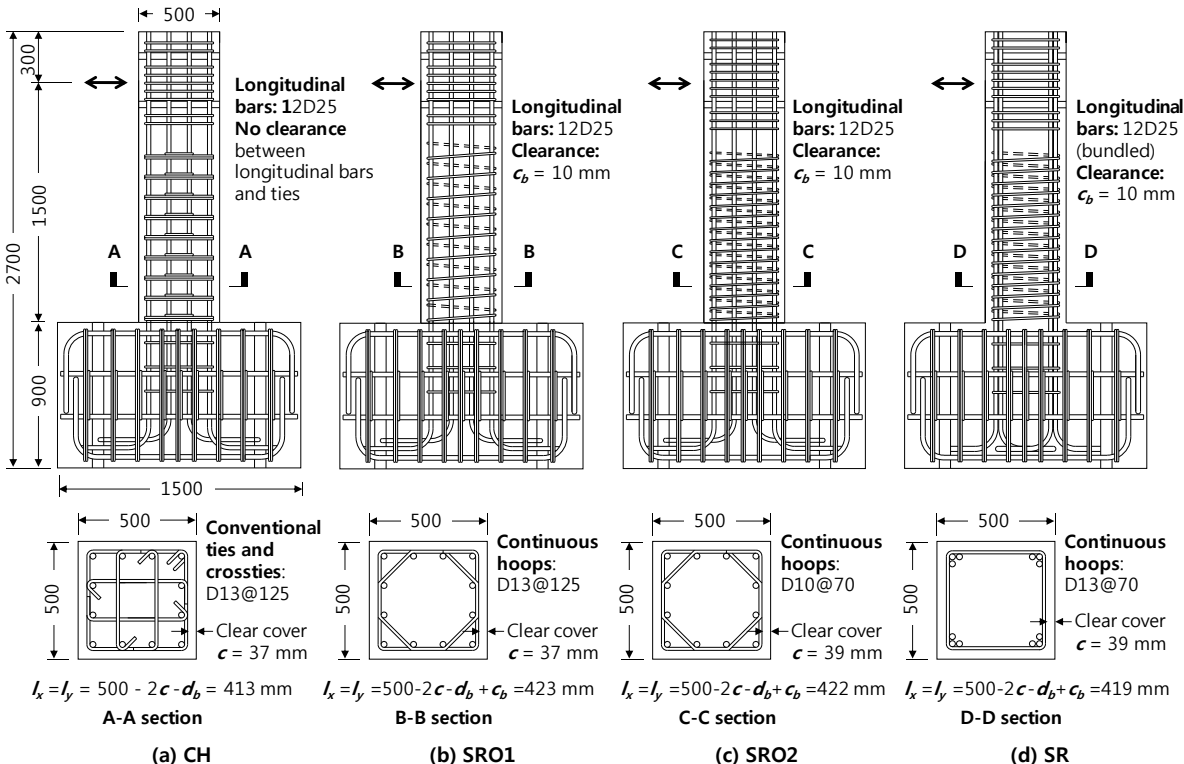


Fig. 3 Configurations, reinforcement details, and cross sections of column specimens

Table 2 Test parameters (mm, mm², and %)

Specimen ⁿ	Longitudinal reinforcement		Transverse reinforcement					
	D_b and No.	Ratio	Detail	d_b and s	A_{sh}	ρ_{sh}	l_h	Bar length ratio ¹
CH	12D25	2.43	Conventional	D13@12 5	508	0.98	4084	-
SRO1	12D25	2.43	Continuous, Detail C	D13@12 5	508	0.96	3090	0.757
SRO2	12D25	2.43	Continuous, Detail C	D10@70	251	0.97	3058	0.749
SR	Bundled 4- 3D25	2.43	Continuous, Detail A	D13@70	254	0.87	1688	0.413

1 The bar length ratios were calculated by dividing the bar lengths l_h of SRO1, SRO2, and SR by l_h of CH.

Fig. 3(a) shows the reinforcement details of specimen CH with conventional ties and crossties. Twelve D25 bars were used for longitudinal bars (reinforcement ratio = 2.43 %). The dimension and spacing of the conventional ties (bar diameter $d_b = 13$ mm) were $l_x \times l_y = 413$ mm x 413 mm and $s = 125$ mm, respectively. The total cross-sectional area of a closed tie including crossties was $A_{sh} = 508$ mm², which was greater than the minimum requirement 406 mm² of ACI 318-11 Sec. 211 (see Table 2). At both ends of the closed ties and crossties, 90° and 135° seismic hooks with $6d_b$ (= 78 mm) extension were used.

Fig. 3(b) shows the reinforcement details and cross section of specimen SRO1 with continuous rectangular-octagonal hoops. The spacing and total cross-sectional area of the continuous hoops were $s = 125$ mm and $A_{sh} = 508$ mm², respectively, which were the same as those of CH with conventional ties and crossties. As presented in Table 2, however, the bar length per hoop was decreased to 75.7 % of the conventional ties and crossties of CH. The locations of longitudinal bars in SRO1 and CH were the same. However, in order to secure a clearance $c_b = 10$ mm between the longitudinal bars and ties for re-bar fabrication work, the continuous hoops of SRO1 were produced in a larger dimension $l_x \times l_y = 423$ mm x 423 mm (see Fig. 3(b)). The actual clear cover of the continuous hoops varied from 27 mm to 37 mm due to the clearance $c_b = 10$ mm, though the nominal clear cover $c = 37$ mm. Fig. 4 illustrates the clearance between the longitudinal bars and the continuous hoops after the re-bar fabrication.

Fig. 3(c) shows the reinforcement details of specimen SRO2 with continuous hoops. SRO2 was considered to investigate the effects of the bar diameter and spacing of the continuous hoops on the earthquake resistance and failure mode of the column. The shape of the continuous hoops was the same as that of SRO1. However, the bar diameter and spacing of the continuous hoops were decreased to $d_b = 10$ mm [0.394 in] and $s = 70$ mm, respectively. By decreasing both the bar diameter and spacing, despite the less area $A_{sh} = 252$ mm² (see Table 2), the continuous hoops of SRO2 had the same volumetric ratio as that of SRO1. As shown in C-C section of Fig. 3(c), the

nominal clear cover of the continuous hoops was increased to $c = 39$ mm due to the less bar diameter of the hoops, as compared with SRO1. The clearance between the longitudinal bars and the tie bars was $c_b = 10$ mm and thus the actual clear cover varied from 29 mm to 39 mm. Thus, the dimension of the continuous hoops in SRO2 was $l_x \times l_y = 422$ mm x 422 mm.

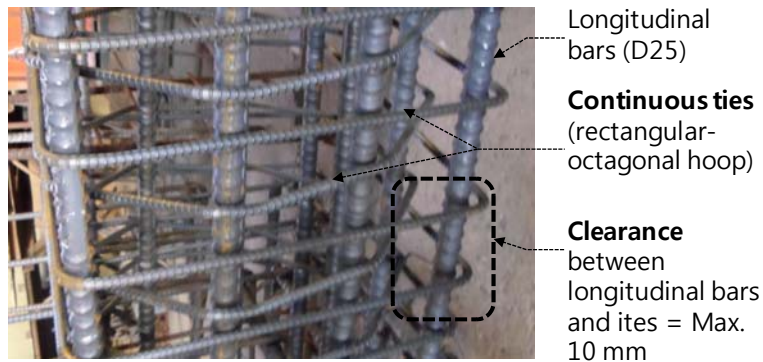


Fig. 4 Clearance between longitudinal bars and continuous hoops (**SRO2**)

Fig. 3(d) shows the reinforcement details of specimen SR with continuous rectangular hoop. Unlike other specimens, bundled 3D25 bars were placed at each corner of the cross section for longitudinal reinforcement so that the flexural capacity of the cross section could be maximized. Since no intermediate longitudinal bar was placed at the edges of the cross section, crossties were not necessary. Thus, the continuous hoops were of a simple form: rectangular hoop. Such ties without crossties may not be applicable to the special moment frames, but satisfy the requirements of the ordinary and intermediate moment frames.

The bar diameter and spacing of the continuous hoops were $d_b = 13$ mm and $s = 70$ mm, respectively. The dimension of the continuous hoops was $l_x \times l_y = 419$ mm x 419 mm, including the clearance $c_b = 10$ mm between the longitudinal bars and tie bars. The cross-sectional area ($A_{sh} = 254$ mm²) of the ties was greater than the requirement ($= 249$ mm²) of ACI 318-11 Sec. 21. The shear reinforcement ratio and the bar length per hoop of SR were 89.3 % and 41.3 % of CH, respectively (see Table 2), which indicates that the tie quantity of SR was only 36.9 % ($= 89.3 \% \times 41.3 \%$) of CH. Thus, the continuous rectangular hoop with the bundled longitudinal bars at the corners was considered as an efficient and economical re-bar arrangement.

The stress-strain relationships of the re-bars are shown in Fig. 5. The yield strength of D25 bars [$D_b = 0.984$ in]) for the longitudinal reinforcement was $f_y = 635$ MPa. The yield strengths of D10 and D13 bars for the ties were $f_y = 572$ and 567 MPa, respectively. The tensile strengths and elongations of D10, D13, and D25 bars were also presented in Fig. 5. The compressive strength of concrete was $f'_c = 34.7$ MPa.

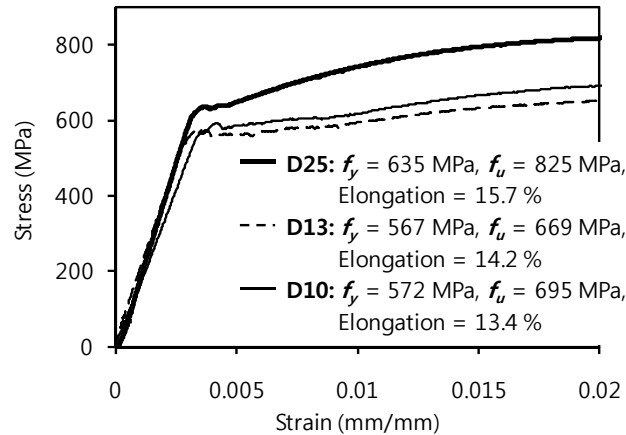


Fig. 5 Stress-strain relationships of reinforcing steel bars by direct tension tests

Fig. 6 shows the loading apparatus and support conditions for cyclic loading test. The column specimens were subjected to a uniform compression $N = 1500$ kN ($= 0.173 A_g f'_c$ where A_g is the cross-sectional area of the columns) during cyclic lateral loading. A lateral load was applied by the 2000 kN actuator. The cyclic loading was controlled by the lateral displacement of the actuator. The load cycles were repeated three times at the lateral drift ratios of 0.25, 0.5, 0.75, and 1.0 %. Then, the lateral drift ratio was increased by 1.3 times of the previous one, repeating the load cycles three times.

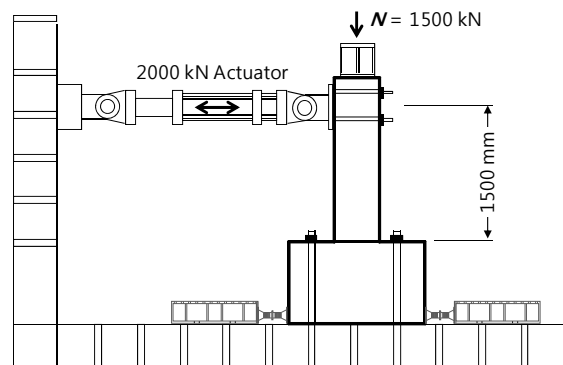


Fig. 6 Test set-up for column specimens

4. TEST RESULTS

4.1 Load-displacement relationships and failure modes

Figs. 7(a) ~ (d) show the lateral load-drift ratio relationships of the column specimens. The lateral drift ratio was calculated by dividing the lateral displacement of the actuator by the net column height (= 1500 mm). Fig. 7(e) shows the envelope curves for the positive and negative loadings. The damages and failure modes at the end of the tests are also shown in Figs. 8(a) ~ (d). The peak strengths P_u , yield drift ratios δ_y , maximum drift ratios δ_u , and displacement ductilities μ ($= \delta_u / \delta_y$) calculated from the envelope curves are presented in Table 3. The values of P_u , δ_y , δ_u , and μ in Table 3 were separately calculated for the positive and negative loadings. The yield drift ratio δ_y was defined as the drift ratio corresponding to the maximum strength P_u , by using the equivalent elastic stiffness connecting the origin and the point of $0.75P_u$, as shown in Fig. 7(f)) (Park 1988). The maximum drift ratio δ_u was defined as the post-peak drift ratio corresponding to $0.75P_u$.

In specimen CH with conventional ties (Fig. 7(a)), flexural yielding occurred at the lateral drift ratios $\delta = \pm 1.2$ %. The peak strengths $P_u = +597$ and -609 kN occurred at $\delta = +2.72$ and -2.66 %, respectively. After the peak strengths, CH showed ductile behavior without significant strength- and stiffness- degradation during cyclic loading. Spalling of cover concrete in the plastic hinge began to occur at $\delta = 2.86$ %, and significant buckling of the longitudinal bars occurred at $\delta = 4.74$ %. Ultimately, CH failed at $\delta = 6.19$ %, due to concrete crushing caused by the failure of the anchorage hooks of the closed ties and crossties (see Fig. 8(a)).

As shown in Fig. 7(b), in SRO1 with continuous rectangular-octagonal hoops (Fig. 7(b)), flexural yielding occurred at $\delta = \pm 1.3$ %. The peak strengths $P_u = +618$ and -607 kN occurred at $\delta = +2.19$ and -4.74 %, respectively. After the peak strengths, the load-carrying capacity decreased due to the spalling of cover concrete and the buckling of longitudinal bars. Ultimately, SRO1 failed at $\delta = 6.19$ %, due to the buckling and fracture of longitudinal bars and the crushing of core concrete (see Fig. 8(b)). Since the bar diameter and spacing of the continuous hoops of SRO1 were the same as those of the conventional ties in CH, the overall cyclic response of SRO1 was similar to that of CH. As shown in Figs. 8(a) and (b), however, the continuous hoops in SRO1 was not fractured even at very large drift ratios, and as a result, the crushing of core concrete was not as significant as CH with the conventional ties and crossties. Although there was a clearance of 10 mm between the longitudinal bars and the ties, the overall structural performance of SRO1 was compatible to that of CH.

In SRO2 with a smaller bar diameter ($d_b = 10$ mm) and a closer spacing ($s = 70$ mm) of continuous hoops, flexural yielding occurred at $\delta = \pm 1.2$ %. The peak strengths $P_u = +597$ and -626 kN occurred at $\delta = +2.05$ and -3.49 %, respectively (see Fig. 7(c)). Spalling of cover concrete and buckling of longitudinal bars began to occur at $\delta = +2.86$ %. After stable cyclic behavior until $\delta = \pm 3.71$ %, SRO2 ultimately failed at $\delta = \pm 4.8$ %, due to the bar fracture of the continuous hoops after the significant buckling of longitudinal bars (see Fig. 8(c)). Although the peak strengths of SRO2 were comparable to those of CH and SRO1, the continuous hoops with the smaller bar diameter $d_b = 10$ mm suffered the fracture failure caused by the out-of-plane displacement of the buckled longitudinal D25 bars. For this reason, the maximum deformation of SRO2 was less than those of CH and SRO1.

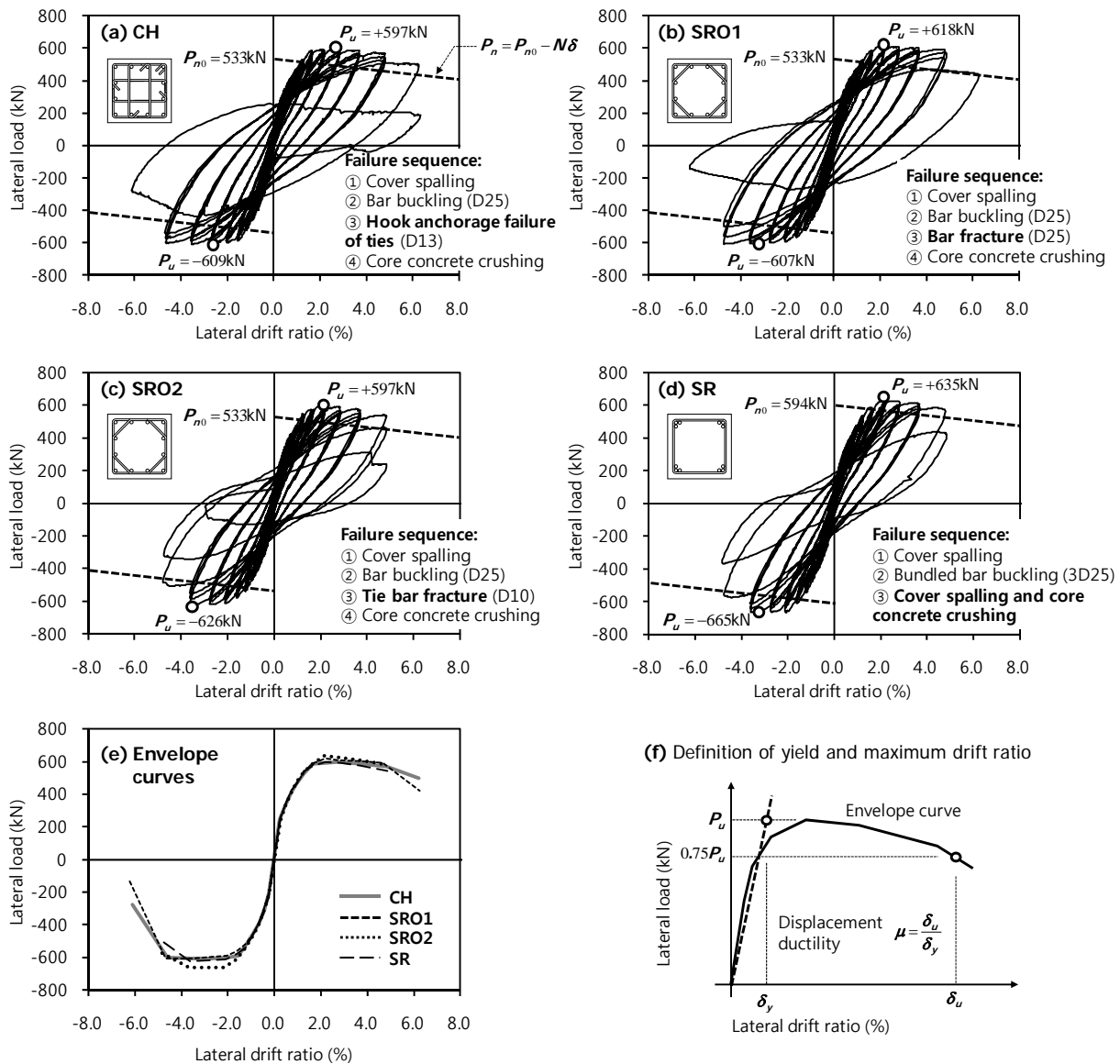


Fig. 7 Lateral load-drift ratio relationships of column specimens

In SR with bundled longitudinal 3D25 bars and continuous rectangular hoops, flexural yielding occurred at $\delta = \pm 1.3\%$. The peak strengths $P_u = +635$ and -665 kN occurred at $\delta = +2.08$ and -2.07% , respectively (see Fig. 7(d)). By placing the bundled longitudinal bars at the corners of the cross-section, the peak strengths of SR were increased by 6.15 ~ 7.78 %, when compared to CH, SRO1, and SRO2. The load-carrying capacity began to decrease after $\delta = \pm 3.71\%$ due to spalling of cover concrete and buckling of longitudinal bars. Ultimately, the specimen failed at $\delta = \pm 4.8\%$ due to significant spalling of cover concrete and crushing failure of core concrete following the buckling of the bundled longitudinal bars (see Fig. 8(d)). The maximum deformation of SR was the same as that of SRO2, but was less than those of CH and SRO1. Although

the amount of the continuous hoops was significantly less than that of SRO2 (compare the bar length per hoop in Table 2), the overall structural performance of SR was similar to that of SRO2. This results indicates that the continuous hoops can be more efficient in strength and tie fabrication, placing the longitudinal bars at the corners of the cross-section. However, in order to secure a higher ductility, it would be desirable to provide intermediate longitudinal bars and crossties as well.

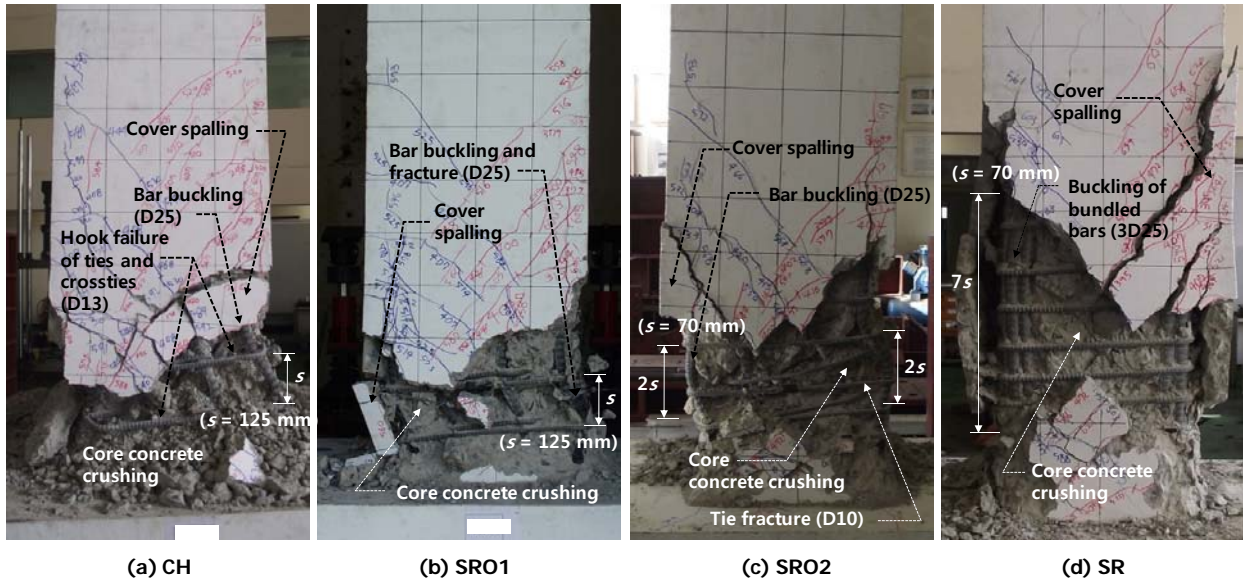


Fig. 8 Failure modes of column specimens

4.2 Strength and ductility

The nominal flexural strength P_{n0} of the column specimens was calculated from a nonlinear section analysis method developed by Eom et al. (2012). The stress-strain relationships of the reinforcing steel bars including the yield strength and strain-hardening in Fig. 5 were used. For the unconfined cover concrete ($f'_c = 34.7$ MPa), a parabolic stress-strain relationship was used. The confinement effects by the transverse ties on the strength and ductility of concrete were addressed by using the Mander's model (1988). The nonlinear section analysis method including the material models of concrete and reinforcing bars were presented in detail in Eom et al. (2012). The maximum lateral load P_{n0} of the specimens was calculated by dividing the flexural moment strength of the critical section, which was obtained from the nonlinear monotonic section analysis, by the net column height 1500 mm. Since the uniform compressive load $N = 1500$ kN was applied, the load-carrying capacity of the columns was modified as $P_n = P_{n0} - N\delta$, addressing the second-order effect. P_n and P_{n0} are the strengths with and without the second-order effect, respectively, and δ is the lateral drift ratio. Figs. 7(a) ~ (d) compare the maximum strengths by the cyclic tests and the nonlinear section analysis. The predicted strengths P_n including the second-order effect

were represented as the dashed lines descending as the lateral drift ratio increases. As shown in the figures, the predicted strengths including the confinement effect by the transverse ties were less than the test results. This result indicates that the nonlinear sectional analysis results for monotonic loading underestimated the post-yield stress of the longitudinal bars increased by the cyclic strain-hardening effect.

Table 3 presents the maximum drift ratios δ_u and displacement ductilities $\mu (= \delta_u / \delta_y)$ of the column specimens. The column specimens subjected to $N = 1500$ kN [337 kips] ($= 0.173 A_g f'_c$) exhibited the maximum drift ratios greater than 4.50 %. The displacement ductility was greater than 3.38. The deformation capacity of SRO1 with continuous hoops was the same as that of CH with conventional closed ties and crossties. However, in SRO2 with smaller bar diameter and spacing (i.e. $d_b = 10$ mm and $s = 70$ mm), the deformation capacity slightly decreased, though the volumetric ratio of the ties was the same as those of CH and SRO1. In addition, in SR with the bundled bars and continuous rectangular hoops, the deformation capacity decreased to the level of SRO2. The decrease in the deformation capacity in SRO2 and SR was associated with the buckling of longitudinal bars, which is discussed in the next sections.

Table 3 Summary of test results (kN and %)

Specime n	Max. strength P_u		Yield drift ratio δ_y		Max. drift ratio δ_u		Ductility μ	
	Positive	Negative	Positive	Negative	Positive	Negative	Positive	Negative
CH	597	609	1.17	1.21	6.19	4.49	5.27	3.70
SRO1	618	607	1.23	1.31	4.75	4.52	3.88	3.46
SRO2	597	626	1.15	1.24	4.83	4.77	4.21	3.84
SR	635	665	1.33	1.38	4.60	4.65	3.46	3.38

4.3 Strains of ties and longitudinal bars

Fig. 9 shows the strains of conventional and continuous ties measured in the plastic hinges of the columns. The vertical and horizontal axes are the lateral drift ratios and the tie strains, respectively. The strain gages were attached to the conventional closed tie and continuous hoops at a height of 250 mm from the column base. As shown in Fig. 9, the strains of the ties continuously increased during cyclic loading in all column specimens. However, even at large lateral drift ratios, the strain of the conventional tie in CH was apparently less than those of the continuous hoops in SRO1, SRO2, and SR: in CH, the strain of the conventional tie was less than the yield strain ($= 0.00284$) because the tie strain did not increase due to the failure of anchorage hook (see Fig. 8(a)); on the other hand, the strains of the continuous hoops in SRO1 and SR ultimately reached the yield strain during crushing of core concrete; and in SRO2 where fracture of the ties occurred, the tie strains increased far beyond the yield strain. Despite such substantial difference in the strains of ties, the cyclic responses of CH, SRO1, and

SRO2 were almost identical, as shown in Fig. 7. This indicates that the deformation capacity of the columns was determined by the buckling of longitudinal bars and the consequent crushing failure of core concrete, rather than the continuity of the ties.

Fig. 10(a) shows the strains of longitudinal bars measured at the plastic hinges of SRO1. The vertical and horizontal axes are the lateral loads and bar strains, respectively. The strain gages were attached to the longitudinal bars at a height of 155 mm from the column base. The strains were measured for $\delta \leq 3.5\%$ because of malfunction of the strain gages. As shown in Fig. 10(a), the longitudinal bars were subjected to large tensile plastic strains during cyclic loading even though the axial compression $N = 1500\text{ kN}$ ($= 0.173 A_g f_c'$) was applied. In the case of the reinforcing bars under a stress reversal from large tensile plastic strains, as illustrated in Fig. 10(b), post-yield buckling can develop earlier than under monotonic compression loading (Rodriguez et al. 1999, Berry and Eberhard 2005, Dhakal and Maekawa 2002). Thus, in the column specimens, the post-yield buckling of the longitudinal bars can precede crushing failure of the core concrete confined by transverse ties. This indicates the buckling of longitudinal bars is primary factor to assess the failure modes and deformation capacities of the column specimens.

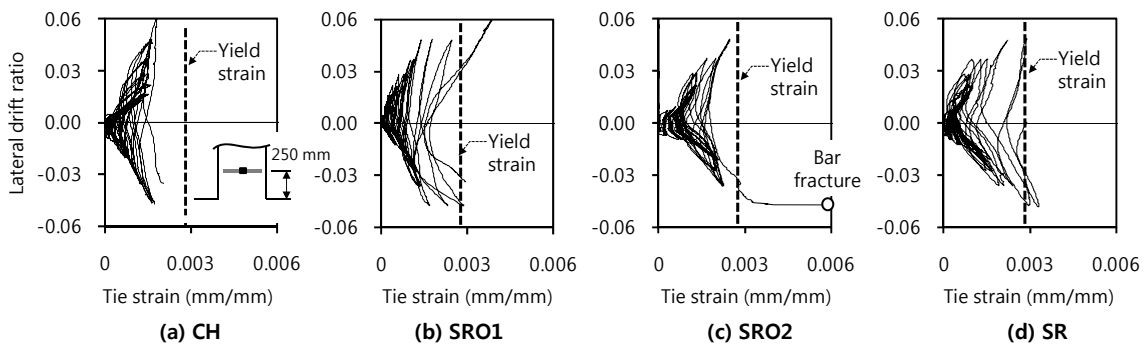


Fig. 9 Strains of conventional and continuous ties

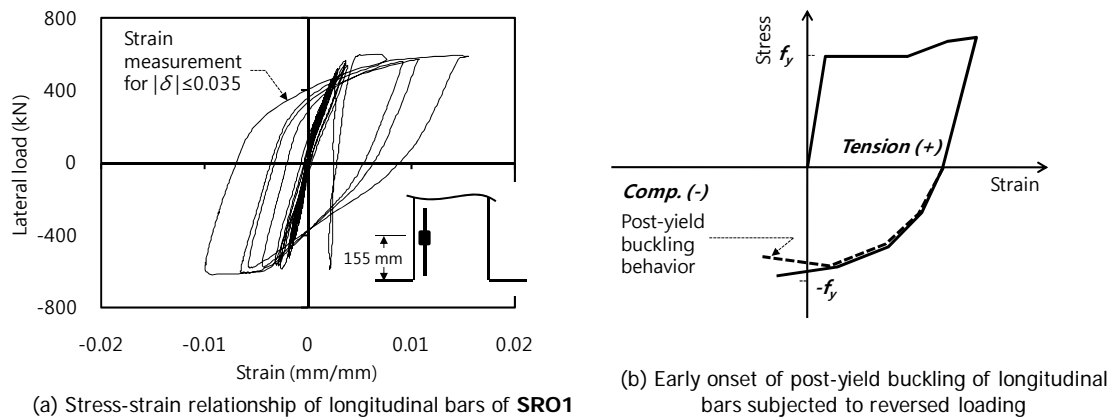


Fig. 10 Early onset of post-yield bar buckling in columns subjected to cyclic loading

4.4 Post-yield buckling of longitudinal bars

As mentioned, the failure of the specimens was initiated by the buckling of the longitudinal bars. The pictures of Fig. 8 show the buckling modes of the longitudinal bars at the end of test, which varied according to the bar diameter and spacing of the continuous hoops. The buckling modes of longitudinal bars were conceptually illustrated in Fig. 11. As shown in Fig. 8(b) and Fig. 11(a), SRO1 with the tie bar diameter $d_b = 13$ mm and the spacing $s = 125$ mm exhibited a non-sway buckling mode of longitudinal bars restrained by two adjacent transverse ties. Approximately, the effective buckling length of the longitudinal bars was the same as the spacing $s = 125$ mm. Despite the buckling of the D25 longitudinal bars, the D13 tie bar of the continuous hoops was not fractured. CH with conventional ties of the same bar diameter and spacing showed the same buckling mode as SRO1 (see Fig. 8(a)). However, the D13 ties and cross-ties were subjected to hook failure due to the out-of-plane displacement of the buckled bars.

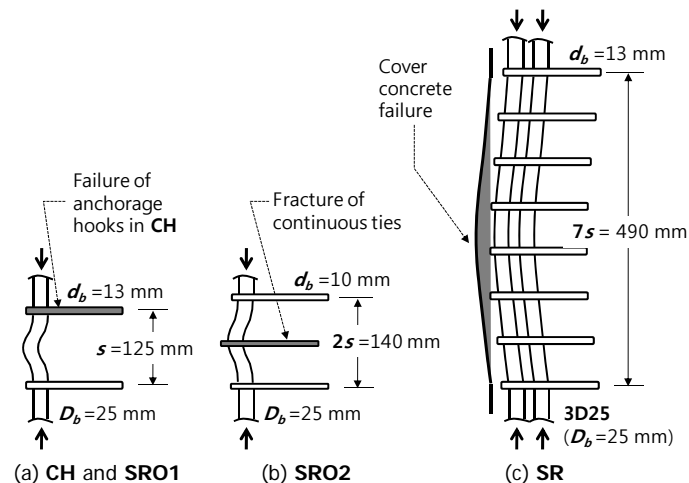


Fig. 11 Buckling modes of longitudinal bars varying with bar diameter and spacing of transverse ties

SRO2 with a smaller bar diameter $d_b = 10$ mm and a smaller spacing $s = 70$ mm, the buckling mode of the longitudinal bars was also non-sway mode, as shown in Fig. 8(c) and Fig. 11(b). However, the effective buckling length was increased to two times the spacing $2s = 140$ mm because the D10 ties did not completely restrain the out-of-plane displacement of the D25 longitudinal bars. Moreover, the D10 continuous hoop ties were fractured at $\delta = +4.8\%$ due to excessive out-of-plane displacement of the buckled bars.

Fig. 11(c) illustrated the buckling mode of the bundled longitudinal bars in SR with closely spaced continuous rectangular hoops. The bar diameter was $d_b = 13$ mm, and the spacing was $s = 70$ mm. Thus, the tie bars successfully restrained a local buckling of the 3D25 bundled bars between two adjacent ties. Instead, the bundled bars were

subjected to a non-sway buckling developing over the buckling length $7s = 490$ mm, as shown in Fig. 8(d) and Fig. 11(c). This is because as compared with SRO1, the out-of-plane force of the bundled bars due to the post-yield buckling was significantly increased. As a result, the spalling of cover concrete occurred over the extended buckling zone of 490 mm.

5. SUMMARY AND CONCLUSIONS

The rectangular or polygonal continuous hoops are an efficient construction method which can reduce construction time and re-bar cost. In the present study, cyclic tests were performed to investigate the structural performance of the columns with continuous hoops. The test parameters were the shape, spacing, and bar-diameter of the continuous hoops, and the tolerance between the longitudinal bars and the ties. The load-carrying capacity, deformation capacity, and failure mode of the specimens were directly compared with those of a column with conventional ties. The major findings are as follows.

- 1) The continuous hoops can be used for diverse sizes and shapes of column cross-sections including rectangular, T-shaped, hexagonal, octagonal, and circular shapes. Since the continuous hoops do not require anchorage hooks, the bar length per hoop can be saved by as much as 25 %, when compared with conventional ties.
- 2) When 13 mm diameter bars with spacing of 125 mm was used for ties, the load-carrying capacity and deformation capacity of the columns with the continuous rectangular - octagonal hoops were the same as those of the column with conventional ties and crossties. The 10 mm clearance between the longitudinal bars and the continuous hoops, which is required for the fabrication of the continuous hoops, did not affect the structural capacity of the column.
- 3) When the continuous rectangular - octagonal hoops with the bar diameter 10 mm and the spacing 70 mm were used for ties, despite the same volumetric ratio of ties, the deformation capacity was decreased due to the bar fracture of continuous hoops. This is because the D10 ties were too small to restrain the out-of-plane displacement of the D25 longitudinal bars growing significantly after post-yield buckling.
- 4) For the column specimen where all longitudinal bars were concentrated only at the corners of the continuous rectangular hoops, the load-carrying capacity was increased by 6.15 to 7.78 %, despite 63.1 % less volume of transverse ties. However, the deformation capacity was decreased. Such re-bar detail may be applicable to the ordinary and intermediate moment frames.

ACKNOWLEDGEMENT

This research was financially supported by DAEHAN STAZ and the Basic Science Research Program through the National Research Foundation of Korea (NRF), funded by the Ministry of Education, Science, and Technology (No. 2012R1A1A1003282). The authors are grateful for their support.

REFERENCES

- ACI Committee 318, Building Code Requirements for Structural Concrete (ACI 318-11) and Commentary, American Concrete Institute, Farmington Hills, MI, 2011.
- Berry, M. P. and Eberhard, M. O., "Practical Performance Model for Bar Buckling", *Journal of Structural Engineering*, ASCE, 131(7), 2005, pp.1060-1070.
- Dhakal, R. P. and Maekawa, K., "Modeling for Postyield Buckling of Reinforcement", *Journal of Structural Engineering*, ASCE, 128(9), 2002, pp.1139-1147.
- Eom, T-S., Hwang, H-J., Park, H-G., Lee, C-N., and Kim, H-S., "Flexural Test for Prefabricated Composite Columns Using Steel Angle and Reinforcing Bar", *Journal of the Korean Society of Steel Construction*, 24(5), 2012, pp.535-547.
- Fascia, F., Chiara, D. M., Piasanti, G., and Iovino, R. Continuous Stirrup with Vertical Arms and Variable Pitch for Reinforced Concrete Structures, Schnell S.p.A. 2010, p.74.
- Korean Concrete Institute, Concrete Structure Design Code (KCI 2012), Korean Concrete Institute, Seoul, pp.324.
- Mander, J. B., Priestley M. J. N., and Park, R., "Theoretical Stress-Strain Model for Confined Concrete," *Journal of Structural Engineering*, ASCE, 114(8), 1988, pp.1804-1826.
- Park, R., "State-of-the-Art Report on Ductility Evaluation from Laboratory and Analytical Testing", *Proceedings of 9th World Conference on Earthquake Engineering*, Tokyo-Kyoto, Japan, 8, 1988, pp.605-616.
- Riva, P., Cyclic Response of Column-to-Foundation Joints with Continuous Stirrups "SPIREX", Schnell Technical Report, 2009, p. 47.
- Rodriguez, M. E., Botero, J. C., and Villa, J., "Cyclic Stress-Strain Behavior of Reinforcing Steel Including Effect of Buckling", *Journal of Structural Engineering*, ASCE, 125(6), 1999, pp.605-612.